ACS OMEGA

http://pubs.acs.org/journal/acsodf

Article

Synergistic Flame Retardant Effect between Ionic Liquid-Functionalized Imogolite Nanotubes and Ammonium Polyphosphate in Unsaturated Polyester Resin

Taohua Zhu, Guozheng Guo, Wanhong Li,* and Ming Gao

Cite This: *ACS Omega* 2022, 7, 47601−47609

Read Online

ACCESS | Metrics & More | Article Recommendations

ABSTRACT: Imogolite nanotubes (INTs) were synthesized from tetraethoxysilane, aluminum nitrate nonahydrate, and ammonia solution by the method of Arancibia-Miranda, and their dispersion was modified by 1-butyl-3-methylimidazolium hexafluorophosphate ([BMIM]PF_6) to obtain ionic liquid (IL)-functionalized INTs (INTs-PF_6-ILs). Then, the flame retardant INTs-PF_6-ILs was complexed with ammonium polyphosphate (APP) and applied to unsaturated polyester resin (UPR). The limiting oxygen index value and the UL-94 level of the UPR/APP/INTs-PF_6-ILs composites reached 28 and V-0, respectively. The residual carbon of the composites in thermogravimetric analysis increased by 19.47%, compared with that of pure UPR. The cone calorimeter test result showed that the peak of heat release rate and total heat rate values of the UPR/APP/INTs-PF_6-ILs composites were lowered by 41 and 34% than those of the pure UPR, respectively. The effect of heat combustion and the maximum mass loss rate of UPR/APP/INTs-PF_6-ILs composites were also greatly decreased. There were no holes or folds observed on the surface of the UPR/APP/INTs-PF_6-ILs composites' residual carbon in scanning electron microscopy images. The intact residual carbon could have effectively insulated the heat and oxygen to improve the flame retardant performance.

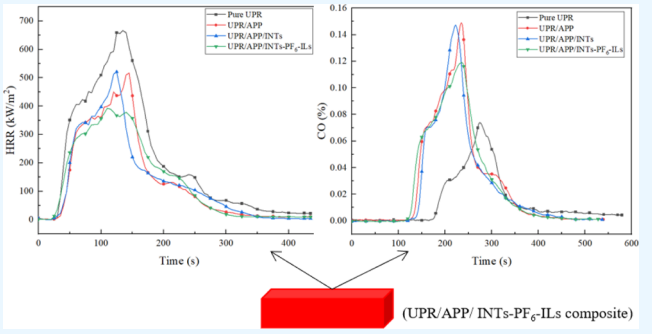

1. INTRODUCTION

Unsaturated polyester resin (UPR) is widely used in different fields, including petroleum, chemical, and mining industries and so forth, because of its outstanding chemical resistance, good mechanical properties, dielectric properties, and low cost.[1] However, UPR is inflammable due to its intrinsic chemical composition and molecular structure,[2] which may cause a fire, limiting its application in many fields.[3] To improve the poor flame retardancy of UPR, many different flame retardants have been invented and used over the past decades, of which the halogen-containing flame retardant is highly effective and is widely used.[4] However, large quantities of smoke and toxic gases are produced during the combustion of the halogenated flame retardant UPR.[5] Therefore, flame retardants tend to be halogen-free compounds, such as phosphorus-containing compounds,[6] aluminosilicate nanoclays,[7] expanded graphite,[8] boron compounds, silicon compounds, and so forth.

Ammonium polyphosphate (APP) is one of the widely used efficient phosphorus−nitrogen flame retardants because APP can act in the pyrolysis of UPR to form an insulating protective layer which prevents further flame spread.[9] Recently, many studies have been done to investigate the synergistic flame retardant effect through introduction of other compounds as synergistic agents into UPR composites.[10] Nano-fillers, such as carbon nanotubes and graphene, are proven to be more effective in improving the flame retardancy of polyolefins.[11−13] Similar to carbon nanotubes, imogolite nanotubes (INTs) are another type of single-walled nanotube materials consisting of hydrous aluminosilicate, having a general formula of $(OH)_3Al_2O_3SiOH$;[14] their outer surface is composed of $Al_2-\mu OH$, while the inner surface is composed of Si−OH[15] and may be a new promising synergistic agent in improving the flame retardancy of UPR.

In this study, INTs were first synthesized by the method of Arancibia-Miranda.[16] Due to the strong interaction between nanoparticles, it is difficult for the INTs to disperse well in organic solvents or hydrophobic polymer matrices.[17] Therefore, to improve the dispersion in UPR, INTs were modified with 1-butyl-3-methylimidazolium hexafluorophosphate ([BMIM]PF_6) and 3-aminopropyltriethoxysilane (KH550) to

Received: May 6, 2022
Accepted: November 28, 2022
Published: December 13, 2022

https://doi.org/10.1021/acsomega.2c02803
ACS Omega 2022, 7, 47601−47609

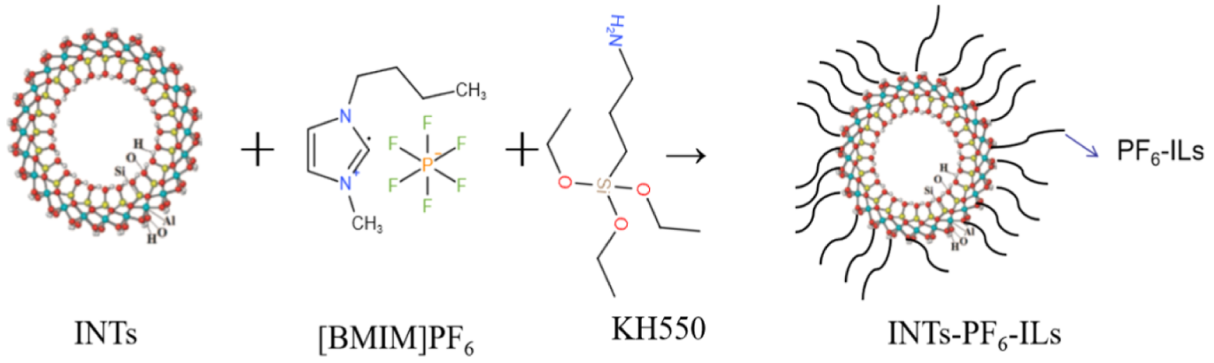

Figure 1. Synthetic schematic of IL -functionalized graphene oxide.

Table 1. Composition of UPR Composites

sample	UPR (wt %)	curing agent (wt %)	accelerator (wt %)	APP (wt %)	INTs (wt %)	INTs-PF_6-ILs(wt %)
pure UPR	94.00	3.00	3.00			
UPR/APP	78.02	2.49	2.49	17		
UPR/APP/INTs	78.02	2.49	2.49	16.6	0.4	
UPR/APP/INTs-PF_6-ILs	78.02	2.49	2.49	16.6		0.4

obtain ionic liquid (IL)-functionalized INTs (INTs-PF_6-ILs). Also, the synergistic effect of INTs-PF_6-ILs and APP on the flame retardancy of UPR was investigated.

2. MATERIALS

Aluminum nitrate nonahydrate [98.0%, $Al(NO_3)_3{\cdot}9H_2O$], sodium hydroxide (98%, NaOH), tetraethyl orthosilicate (TEOS), and ammonia solution (25%, $NH_3{\cdot}H_2O$) were obtained from Tianjin Yongda Chemical Reagent Co., Ltd. (China). 3-Aminopropyltriethoxysilane [$(C_2H_5O)_3{-}Si{-}(CH_2)_3NH_2$, 97%, AR] was bought from Nanjing Shuguang Chemical Group Co., Ltd. (China). 1-*N*-Butyl-3-methylimidazolium hexafluorophosphate ([BMIM]PF_6, AR) was produced by Linzhou Keneng Material Technology Co., Ltd. (China). Anhydrous ethanol (C_2H_5OH, 98%, AR) was furnished by Jiangsu Qiangsheng Functional Chemical Co., Ltd. (China). UPR (191), curing agent, and accelerator were of industrial grade and obtained from Henan Zhongyi Yiyuan Chemical Co., Ltd. (China). APP was provided by Tangshan Yongfa Flame Retardant Material Factory (China).

2.1. Preparation of INTs. The synthesis of INTs followed the method of Arancibia-Miranda et al.[16] Sources of Si and Al in the INTs are from TEOS and $Al(NO_3)_3{\cdot}9H_2O$. $Al(NO_3)_3{\cdot}9H_2O$ aqueous solution with a concentration of 5×10^{-3} mol/L was prepared. An appropriate amount of TEOS was added into an aqueous solution of $Al(NO_3)_3{\cdot}9H_2O$ to get a final mixed solution with a Si/Al mole ratio of 0.5. The above-mixed solution was stirred vigorously at room temperature for 1 h. 1×10^{-2} mol/L of NaOH solution was added into the mixed solution of TEOS and $Al(NO_3)_3{\cdot}9H_2O$ until the molar ratio of Al/Si/OH was 2:1:4. Then, the mixed solution was stirred vigorously at room temperature for 1 h in a pH of 5. The mixed solution was heated at 95 °C for 6 days. After the solution was cooled to room temperature, the pH of the solution was adjusted to 8 with an aqueous solution of $NH_3{\cdot}H_2O$. The solution was centrifuged at 8000 rpm for 10 min to obtain a gel. The gel was freeze-dried and ground to obtain INT powder.

2.2. Preparation of INTs-PF_6-ILs. The synthesis of INTs-PF_6-ILs followed the method of Wan et al.[18] At first, 0.2 g of prepared INTs was added to 50 mL of 98% ethanol solution. The solution was ultrasonically dispersed for 20 min. Then, 1 mL of [BMIM]PF_6 and 20 mL of deionized water were put in the solution. Two drops of KH550 were added to the solution. The solution was stirred magnetically for 1 h after it was heated to 50 °C. At last, the solution was filtered, washed with anhydrous ethanol and deionized water, dried, and ground to acquire INTs-PF_6-ILs. The schematic diagram of INTs-PF_6-ILs synthesis is shown in Figure 1.

2.3. Preparation of UPR Composites. The composition of UPR composites is shown in Table 1. First, the flame retardant (APP, INTs, or INTs-PF_6-ILs) was dispersed in the UPRs under mechanical agitation treatment for 30 min. Then, a curing agent and an accelerator were added to the mixture. Finally, the mixture was agitated for 5 min, placed in an aluminum mold, and solidified.

2.4. Characterization of INTs and INTs-PF_6-ILs. *2.4.1. Fourier Transform Infrared Spectroscopy Analysis.* Fourier transform infrared (FTIR) spectra of the samples were obtained on an FTS 2000 FTIR (Varian). INTs were mixed with KBr in a ratio of 1:200, ground, and pressed into a sheet. Spectra ranging from 400 to 4000 cm^{-1} were obtained by accumulating 64 scans at a resolution of 1 cm^{-1}.

2.4.2. Transmission Electron Microscopy. The morphology of INTs was characterized by transmission electron microscopy (TEM) (JEM-2010, Japan). INTs were dispersed in alcohol for 30 min by ultrasonication. The dispersed INTs and INTs-PF_6-ILs were placed in the net and dried naturally in the air. The acceleration voltage of the instrument was 200 kV during testing.

2.4.3. Energy-Dispersive Spectroscopy. The elemental composition of INTs and INTs-PF_6-ILs was analyzed by a PE2400 elemental microanalyzer (USA).

2.5. Measurement and Characterization of UPR Samples. *2.5.1. Limiting Oxygen Index.* The limiting oxygen index (LOI) value was analyzed with a JF-3 oxygen index instrument (Jiangning Analysis Instrument Co., Ltd., China) according to ASTMD 2863-2000. Each sample size was $130 \times 6.5 \times 3$ mm^3.

https://doi.org/10.1021/acsomega.2c02803
ACS Omega 2022, 7, 47601−47609

2.5.2. UL-94. The vertical burning test was done with a CZF-3 instrument (Jiangning Analysis Instrument Co., Ltd., China) according to ASTMD 3801. Each sample size was 100 × 10 × 3 mm^3.

2.5.3. Thermogravimetric Analysis. Thermogravimetric analysis (TGA) of UPR composites using an HCT2 instrument (Beijing Hengjiu Scientific Instrument Factory) was carried out under the conditions of air atmosphere and cold tap water. The weight of UPR composites was controlled in the range of 5−10 mg. The temperature was increased from 50 to 800 °C, and the heating rate was 15 °C/min.

2.5.4. Cone Calorimeter Test. The cone calorimeter test (CCT) was conducted by a PX-07-007 instrument (Phoenix Quality Inspection Instrument Co., Ltd.). All sample sizes were 100 × 100 × 4 mm^3. The samples, wrapped in an aluminum foil, were placed in the instrument, whose heat radiation was adjusted to 50 $kW{\cdot}m^{-2}$.

2.5.5. Scanning Electron Microscopy. The carbon residue was studied by scanning electron microscopy (SEM, KYKY-EM3200, Beijing Zhongke Keyi Co., Ltd.) after the CCT. The accelerating voltage at the time of the experiment was 22 kV.

3. RESULTS AND DISCUSSION

3.1. FTIR Spectroscopy. The FTIR absorption spectra of INTs and INTs-PF_6-ILs are shown in Figure 2. The absorption

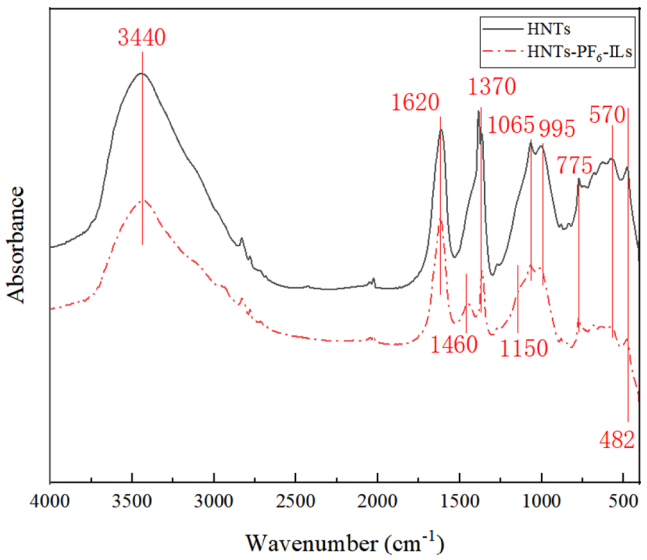

Figure 2. FTIR spectra of INTs and INTs-PF_6-ILs.

band at 3440 cm^{-1} corresponds to the stretching vibrations of OH in INTs and INTs-PF_6-ILs.[17] The peaks at 570 and 775 cm^{-1} correspond to the stretching of the O−Si−O and O−Al−O bonds, respectively.[19] The band at 482 cm^{-1} is associated with the bending vibrations of O−Si. The absorption bands at 1065 and 995 cm^{-1} were attributed to the stretching vibration of Si−O−Al in INTs and INTs-PF_6-ILs.[20] The new band observed at 1460 cm^{-1} corresponds to the bending vibration of $-CH_2$ groups in INTs-PF_6-ILs.[21] The peak at 1150 cm^{-1} corresponds to the P−O bond in INTs-PF_6-ILs.[18] The reason might be that the silanol (Si−OH) produced by hydrolysis of KH550 reacts with the P−F bond in [BMIM]PF_6, which shows that the surface of INTs is grafted with the element P of [BMIM]PF_6. Therefore, INTs have been successfully synthesized and modified with KH550 and [BMIM]PF_6 to obtain INTs-PF_6-ILs.

3.2. EDS and TEM. The element compositions of INTs and INTs-PF_6-ILs are shown in Figure 3. The unique elements of aluminum, oxygen, and silicon in INTs are shown in Figure 3A. The unique elements of carbon, phosphorus, and fluorine in INTs-PF_6-ILs are shown in Figure 3B. The result indicates that INTs have been successfully synthesized and modified with KH550 and [BMIM]PF_6 to obtain INTs-PF_6-ILs.

The tubular structures of INTs and INTs-PF_6-ILs are directly confirmed by TEM observations. From Figure 3A, it can be seen that INTs are stacked together, not scattered at all, while INTs-PF_6-ILs are well dispersed, and their tubular structure can be clearly seen in Figure 3B. The uniformly dispersed INTs-PF_6-ILs appear in as a spidery network consisting of individual fibers in TEM images. The fibers are approximately 100−200 nm in length. The fibers are about 10−20 nm in diameter. The structures and lengths of INTs and INTs-PF_6-ILs show that INTs have been successfully synthesized, and their dispersion is greatly modified by [BMIM]PF_6.

3.3. LOI and UL-94 of UPR Composites. The LOI is the minimum percentage of oxygen that is required to continue the flaming combustion of a sample under laboratory conditions.[22] UL-94 test is one of the most used tests in the field of flame retardancy of polymeric materials.[23] As shown in Table 2, LOI values of pure UPR, UPR/APP composites, UPR/APP/INTs composites, and UPR/APP/INTs-PF_6-ILs composites are 20.8, 25.8, 27.2, and 28, respectively. The LOI values of UPR/APP composites, UPR/APP/INTs composites, and UPR/APP/INTs-PF_6-ILs composites have increased by about 28, 34, and 38%, compared with pure UPR, respectively. The UL-94 result of UPR/APP/INTs-PF_6-ILs composites reaches the V-0 level, while UPR/APP composites and UPR/APP/INTs composites reach the V-2 level and V-1 level. The data in Table 2 proves that the flame retardant performance of UPR/APP/INTs composites and UPR/APP/INTs-PF_6-ILs composites has been obviously improved and INTs-PF_6-ILs has better synergistic flame retardancy with APP in UPR, compared with INTs.

3.4. Thermogravimetric Analysis. TGA is often used to evaluate the thermal stability of the materials, which is mainly related to the decomposition temperature and char yield.[24] In this experiment, the temperature corresponding to 5% weight loss was used as the initial decomposition temperature (T_i) of UPR samples. T_{max} is the temperature corresponding to the maximum weight loss rate.

The T_i of pure UPR is 290 °C, as shown in Table 3. The decomposition of pure UPR has three steps mainly. Pure UPR loses weight rapidly from 200 to 400 °C in the first step because the oxygen-containing groups in it decompose into CO, CO_2, and H_2O. Weight loss of pure UPR occurs from 450 to 540 °C in the second step because of the chain scission of polystyrene and polyester fragment.[25] Slight weight loss of pure UPR occurs from 550 to 630 °C in the third step because the carbon skeleton formed at high temperatures is decomposed by oxidation in the air.

The T_i values of UPR/APP composites, UPR/APP/INTs composites, and UPR/APP/INTs-PF_6-ILs composites are increased by 16, 12, and 12 °C, respectively, compared with pure UPR. The data proves that with the addition of APP, INTs, or INTs-PF_6-ILs, the thermal stability of UPR composites is increased. Except for pure UPR, the decom-

https://doi.org/10.1021/acsomega.2c02803
ACS Omega 2022, 7, 47601−47609

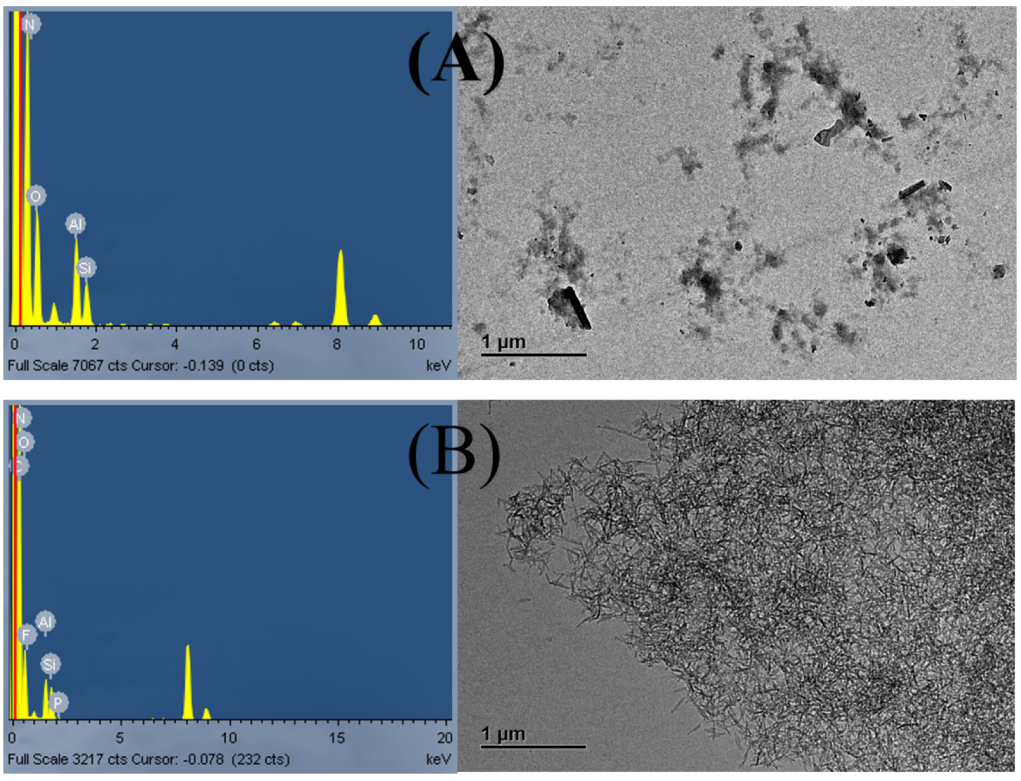

Figure 3. (A) Elemental compositions and TEM images of INTs. (B) Elemental compositions and TEM images of INTs-PF_6-ILs.

Table 2. LOI and UL-94 of UPR Composites

samples	LOI (%)	UL-94
pure UPR	20.8 ± 0.1	
UPR/APP	25.8 ± 0.2	V-2
UPR/APP/INTs	27.2 ± 0.1	V-1
UPR/APP/INTs-PF_6-ILs	28 ± 0.1	V-0

Table 3. TGA Data of UPR Composites

	air atmosphere		
sample	T_i (°C)	T_{max} (°C)	residue at 730 °C (%)
pure UPR	290	370	9.83
UPR/APP	306	343	28.2
UPR/APP/INTs	302	339	30.8
UPR/APP/INTs-PF_6-ILs	302	340	29.3

position of the other three groups of samples also has three steps, which are 200−400, 500−600, and 650−730 °C, as shown in Figures 4 and 5. The peak of UPR/APP/INTs-PF_6-ILs composites' deriv. weight is 1%/°C, the smallest among all the samples. The peaks of other samples' deriv. weight are lower than that of pure UPR in the first step because APP can decompose into polyphosphoric acid and ammonia during combustion,[26] the polyphosphoric acid can react with a hydroxyl group or other groups of synergists to form a nonstable phosphate ester,[27] and dehydration of phosphate ester with the temperature increase will form residual carbon to reduce weight loss rate on the surface of UPR composites.[28] Pure UPR's deriv. weight reaches its peak much earlier than other samples in the second and third steps. This shows that the thermal stability of pure UPR is poor. The residual carbon rates of UPR/APP composites, UPR/APP/INTs composites, and UPR/APP/INTs-PF_6-ILs composites are increased by

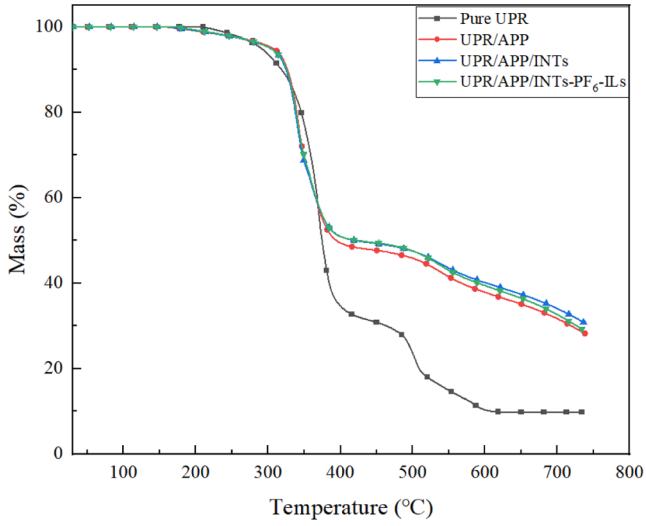

Figure 4. TGA curves of UPR composites.

18.37, 20.97, and 19.47%, respectively, as shown in Table 3, compared with pure UPR.

3.5. Cone Calorimeter Test. The cone calorimeter is one of the most important and widely used instruments for the research and development of fire-retardant polymeric materials.[29] The characteristic data tested by the cone calorimeter is shown in Figures 6−9 and Table 4.

As shown in Figure 6 and Table 4, the peak heat release rate (PHRR) value of pure UPR is 666.25 kW·m^{-2}, the highest among all the samples. The PHRR value of UPR/APP/INTs-PF_6-ILs composites is 392.46 kW·m^{-2}, the lowest among all the samples. The PHRR values of UPR/APP composites and UPR/APP/INTs composites are respectively 516.68 and

https://doi.org/10.1021/acsomega.2c02803
ACS Omega 2022, 7, 47601−47609

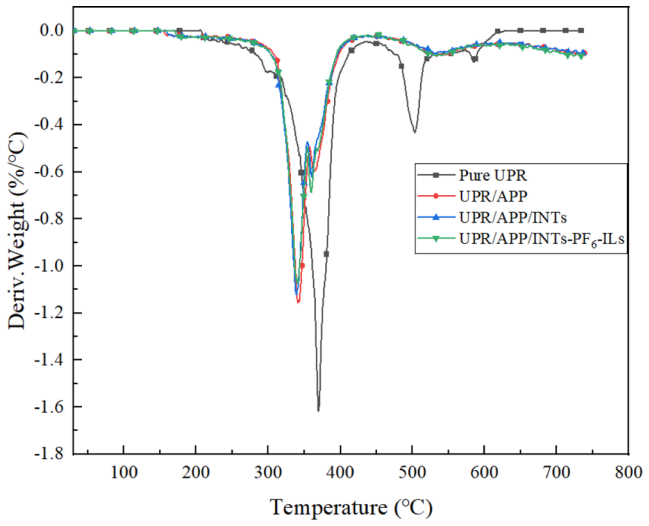

Figure 5. Derivative thermogravimetric curves of UPR composites.

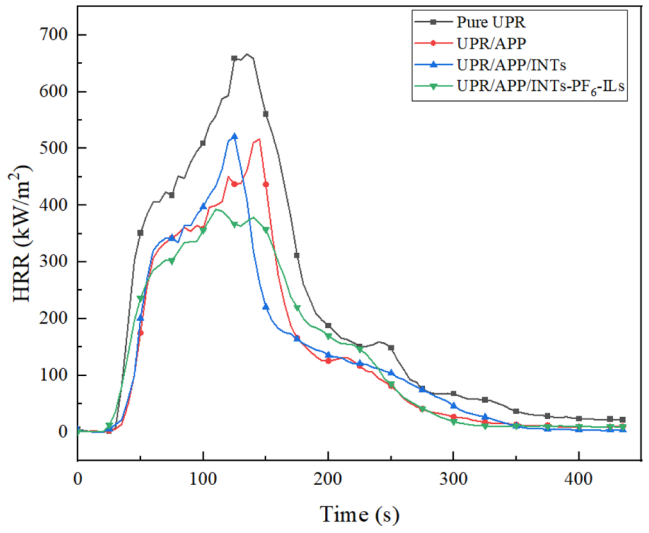

Figure 6. HRR curves of UPR composites.

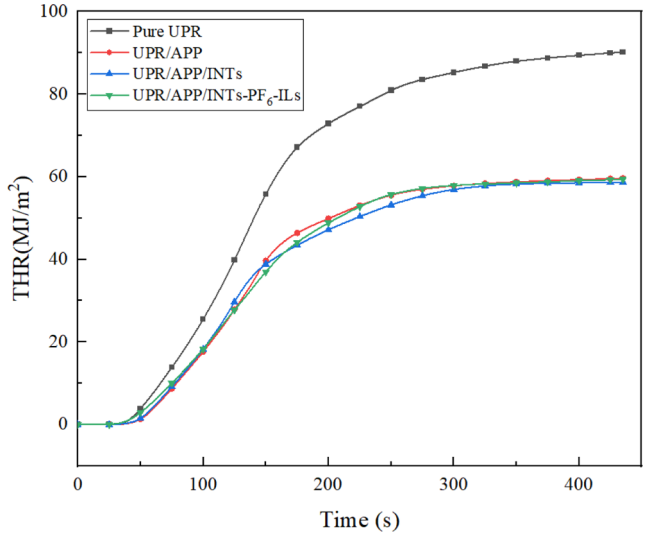

Figure 7. THR curves of UPR composites.

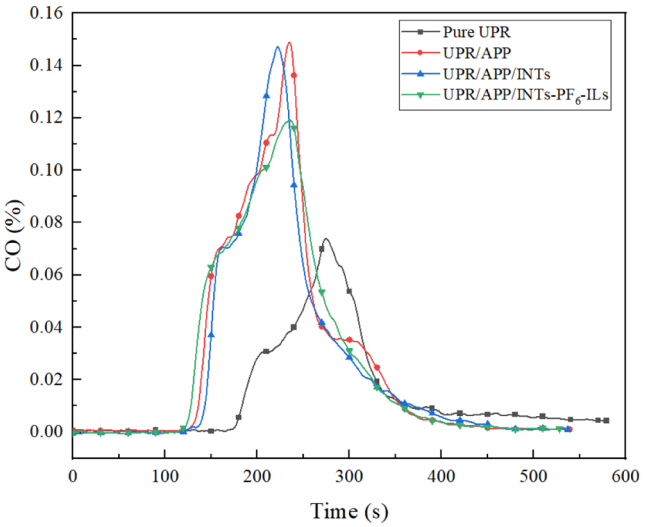

Figure 8. Y_{CO} curves of UPR composites.

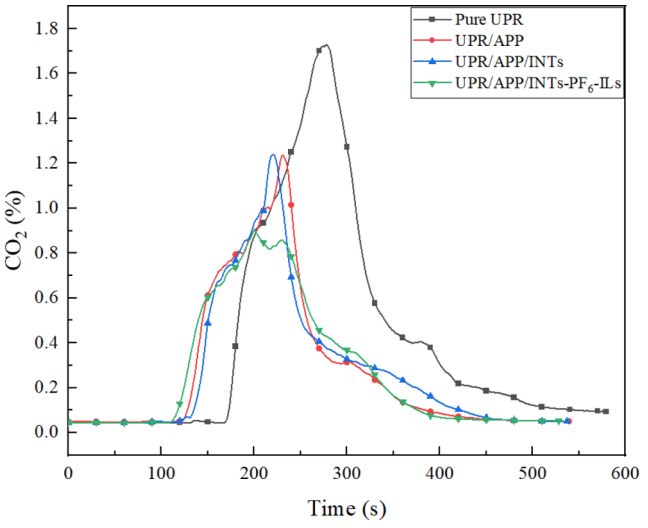

Figure 9. Y_{CO_2} curves of UPR composites.

520.65 kW·m^{-2}. The times taken to reach PHRR values of pure UPR, UPR/APP composites, UPR/APP/INTs composites, and UPR/APP/INTs-PF$_6$-ILs composites are 132, 145, 125, and 110 s, respectively. The time taken to reach the PHRR value of UPR/APP/INTs-PF$_6$-ILs composites is the lowest among all the samples and 22 s less than that of pure UPR. The reason for the phenomenon is the catalytic effect of INTs-PF$_6$-ILs on carbonization to form a protective carbon layer during the combustion of UPR/APP/INTs-PF$_6$-ILs composites, which will isolate the substrate from oxygen and heat. The result suggests that INTs-PF$_6$-ILs have better synergistic flame retardancy with APP in UPR, compared with INTs.

The fire performance index (FPI) is explained as the TTI divided by the PHRR.[30] The higher the FPI value of a sample, the lower the fire risk. The fire spread index (FSI) was the ratio of PHRR to T_{PHRR}.[31] These formulas are as follows

$$FPI = TTI/PHRR$$

$$FSI = PHRR/T_{PHRR}$$

https://doi.org/10.1021/acsomega.2c02803
ACS Omega 2022, 7, 47601−47609

Table 4. Characteristic Data Tested by a Cone Calorimeter

sample	pure UPR	UPR/APP	UPR/APP/INTs	UPR/APP/INTs-PF_6-ILs
TTI (s)	32	36	43	29
PHRR ($kW·m^{-2}$)	666.25	516.68	520.65	392.46
time to PHRR (s)	132	145	125	110
THR ($kW·m^{-2}$)	90.12	59.61	58.30	59.32
av-Y_{CO} (%)	0.037	0.082	0.080	0.080
av-Y_{CO_2} (%)	1.56	1.103	1.135	1.074
FPI	0.048	0.069	0.083	0.073
FSI	5.047	3.563	4.165	3.57
EHC ($MJ·kg^{-1}$)	18.904	15.017	14.956	14.701
MLR ($g·s^{-1}$)	0.104	0.087	0.087	0.087

The FPI values of pure UPR, UPR/APP composites, UPR/APP/INTs composites, and UPR/APP/INTs-PF_6-ILs composites are 0.048, 0.069, 0.083, and 0.073. The FPI value of UPR/APP/INTs-PF_6-ILs composites is 52% higher than that of pure UPR. The fire risk of UPR/APP/INTs-PF_6-ILs composites has been greatly reduced, and its flame retardant performance has been greatly improved. The FSI values of pure UPR, UPR/APP composites, UPR/APP/INTs composites, and UPR/APP/INTs-PF_6-ILs composites are 5.047, 3.563, 4.165, and 3.57. The FSI value of pure UPR is the highest among all the samples, and its fire risk is the highest. The flame retardant performance of UPR composites with APP and INTs-PF_6-ILs has been greatly improved.

The total heat release (THR) curves and values of UPR composites are shown in Figure 7 and Table 4. In Figure 7, the THR curve of pure UPR is going up the fastest among all the samples. This phenomenon shows that it only takes a very short time for pure UPR to reach the state of intense combustion. The THR values of pure UPR, UPR/APP composites, UPR/APP/INTs composites, and UPR/APP/INTs-PF_6-ILs composites are 90.12, 59.61, 58.30, and 59.32 $kW·m^{-2}$, respectively. The THR value of UPR/APP/INTs-PF_6-ILs composites is 34% lower than that of pure UPR. The smaller the THR value of composites is, the less they burn.

The maximum mass loss rate (MLR) of pure UPR is the largest in all samples. The effect of heat combustion (EHC) reflects the burning degree of the combustible and volatile gas in the gas phase.[32] The smaller the EHC value, the smaller the flame. From Table 4, it can be seen that EHC values of UPR/APP composites and UPR/APP/INTs composites are decreased by 3.887 and 3.948 $MJ·kg^{-1}$, respectively, compared with pure UPR. The EHC value of UPR/APP/INTs-PF_6-ILs composites is decreased by 4.203 $MJ·kg^{-1}$, compared with pure UPR. The result proves that INTs-PF_6-ILs have better synergistic flame retardancy with APP in UPR, compared with INTs.

When the oxygen concentration in the combustion zone is insufficient, the combustion produces includes both complete (CO_2, H_2O, and acid gases) and incomplete (soot, CO, and partially oxidized volatile fuels) combustion products.[33] The higher the av-CO yield (Y_{CO}) value and the lower the av-CO_2 yield (Y_{CO_2}) value are, the less the combustion of UPR there is. However, the higher the av-CO yield (Y_{CO}) value is, the more harmful it is. The av-Y_{CO} values of pure UPR, UPR/APP composites, UPR/APP/INTs composites, and UPR/APP/INTs-PF_6-ILs composites are 0.037, 0.082, 0.080, and 0.080%, as shown in Table 4. The av-Y_{CO} values of UPR/APP/INTs composites and UPR/APP/INTs-PF_6-ILs composites are lower than that of UPR/APP composites, and UPR/APP/INTs-PF_6-ILs composites have the third highest peak Y_{CO} values of all samples shown in Figure 8. Therefore, the combustion of UPR/APP/INTs-PF_6-ILs composites is the least sufficient, and its peak Y_{CO} value is decreased. The av-Y_{CO_2} values of pure UPR, UPR/APP composites, UPR/APP/INTs composites, and UPR/APP/INTs-PF_6-IL composites are 1.56, 1.103, 1.135, and 1.074%, as shown in Table 4. The av-Y_{CO_2} value of the UPR/APP/INTs-PF_6-ILs composites is the lowest among all the samples and 0.486% higher than that of pure UPR, as shown in Table 4. The peak Y_{CO_2} value of UPR/APP/INTs-PF_6-ILs composites is the lowest among all the samples in Figure 9. The result proves that INTs-PF_6-ILs have good CO and CO_2 suppression in UPR.

As shown in Figure 10, the peak surface plasmon resonance (SPR) values of pure UPR, UPR/APP composites, UPR/APP/INT composites, and UPR/APP/INTs-PF_6-ILs composites are 0.164 m^2/s in 140 s, 0.199 m^2/s in 155 s, 0.187 m^2/s in 135 s, and 0.191 m^2/s in 130 s respectively. The peak SPR values of UPR/APP composites, UPR/APP/INTs composites, and UPR/APP/INTs-PF_6-ILs composites are increased by 21, 14, and 14%, compared with pure UPR, respectively.

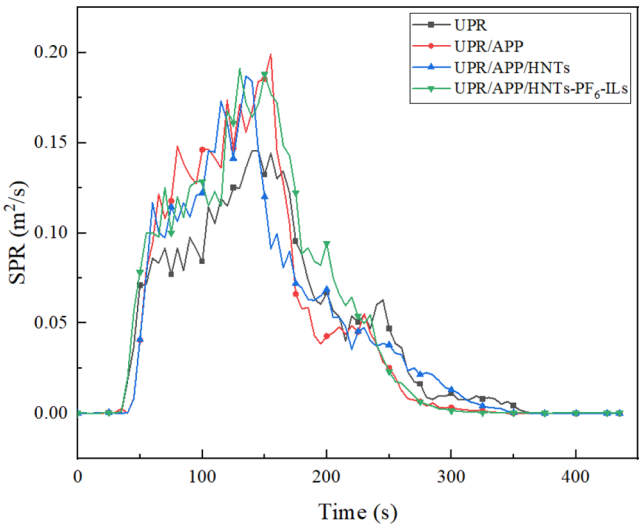

Figure 10. SPR curves of UPR composites.

3.6. Scanning Electron Microscopy. Figure 11 displays SEM images of residual carbon of pure UPR, UPR/APP composites, UPR/APP/INTs composites, and UPR/APP/INTs-PF_6-ILs composites. The surface of pure UPR's residual carbon has many holes of different diameters and small

https://doi.org/10.1021/acsomega.2c02803
ACS Omega 2022, 7, 47601−47609

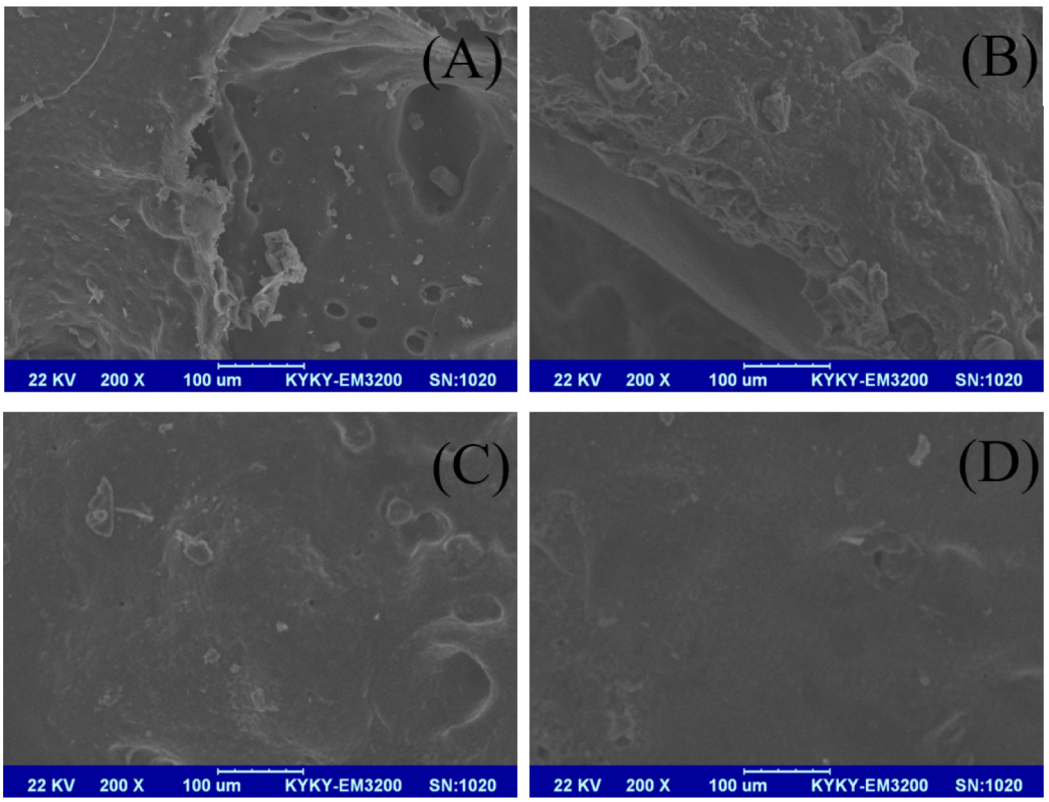

Figure 11. SEM images of UPR composites' residual carbon: (A) pure UPR, (B) UPR/APP composites, (C) UPR/APP/INTs composites, and (D) UPR/APP/INTs-PF_6-ILs composites.

fragments of different sizes, as shown in Figure 11A. This phenomenon shows that the carbon layer formed when pure UPR burns is brittle, porous, and unable to effectively insulate itself from oxygen and heat. There are a lot of fluffy and uneven floccule structures on the surface of UPR/APP composites' residual carbon, as shown in Figure 11B. The strength of the floccule carbon layer is poor, so the gas generated by UPR/APP composites' combustion easily breaks through the carbon layer and forms small cavities. Heat and oxygen will enter the residual carbon through these little cavities and cause UPR/APP composites inside to continue to burn. The surface of the UPR/APP/INTs composites' residual carbon has a small number of holes and similar-sized particles, as shown in Figure 11C. The carbon layer of UPR/APP/INTs composites has high strength and is not easily broken due to the addition of INTs. The surface of UPR/APP/INTs-PF_6-ILs composites' residual carbon has fewer wrinkles, holes, and particles, as shown in Figure 11D, compared with other samples, because INTs-PF_6-ILs uniformly disappeared in the UPR, and the phosphorus in INTs helps the UPR form carbon during combustion. These UPR/APP/INTs-PF_6-ILs composites' residual carbon with intact surfaces can be well insulated from heat and oxygen to improve their flame retardant properties. Figure 10 proves that INTs-PF_6-ILs have better synergistic flame retardancy with APP in UPR.

4. CONCLUSIONS

INTs-PF_6-ILs with good dispersion were successfully synthesized as good synergistic agents compounded with APP, which greatly improved the flame retardancy of UPR composites, whose LOI value and the UL-94 level reach 28 and V-0, respectively, and the residual carbon in the TGA is 29.3%.

APP mainly acts in the condensed phase to form residual carbon and reduce the weight loss rate on the surface of UPR composites, while INTs-PF_6-ILs catalyze carbonization to form a strong intact carbon layer during the combustion of the UPR composites, which could effectively isolate the substrate from oxygen and heat. The result suggests that INTs-PF_6-ILs have good synergistic flame retardancy with APP in UPR.

For the UPR/APP/INTs-PF_6-ILs composites, CCT results showed the MLR, heat release rate, THR, and the time taken to reach PHRR value were greatly decreased. The FPI and FSI values of UPR/APP/INTs-PF_6-ILs composites increased by 52% and decreased by 29.2%, respectively, compared with pure UPR, which showed that its fire risk was much decreased. Meanwhile, INTs-PF_6-ILs showed good smoke, CO, and CO_2 suppression for the UPR composites.

AUTHOR INFORMATION

Corresponding Author

Wanhong Li − *College of Innovation and Entrepreneurship, Kunming Metallurgy College, Kunming, Yunnan Province 650033, China;* orcid.org/0000-0003-2299-4061; Email: wanhonglikm@foxmail.com

Authors

Taohua Zhu − *Department of Chemistry and Chemical Engineering, School of Chemistry and Biological Engineering, University of Science and Technology Beijing, Beijing 100083, China; School of Electronic Science and Control Engineering, Institute of Disaster Prevention, Sanhe 065201, China*

Guozheng Guo − *School of Chemistry and Environmental Engineering, North China Institute of Science and Technology, Beijing 101601, China*

https://doi.org/10.1021/acsomega.2c02803
ACS Omega 2022, 7, 47601−47609

Ming Gao − *School of Chemistry and Environmental Engineering, North China Institute of Science and Technology, Beijing 101601, China;* orcid.org/0000-0001-7936-9895

Complete contact information is available at: https://pubs.acs.org/10.1021/acsomega.2c02803

Notes

The authors declare no competing financial interest.

■ ACKNOWLEDGMENTS

This work was supported by the Open Project Program from the Petroleum and Chemical Industry Engineering Laboratory of Nonhalogen Flame Retardants for Polymers (grant no. BTBUFR21-3), Beijing Technology and Business University, China, and the Natural Science Foundation of Hebei Province (B2020508008).

■ REFERENCES

(1) Hou, Y.; Hu, W.; Gui, Z.; Hu, Y. Effect of Cuprous Oxide with Different Sizes on Thermal and Combustion Behaviors of Unsaturated Polyester Resin. *J. Hazard. Mater.* **2017**, *334*, 39−48.

(2) Chen, Z.; Jiang, M.; Chen, Z.; Chen, T.; Yu, Y.; Jiang, J. Preparation and Characterization of a Microencapsulated Flame Retardant and Its Flame-Retardant Mechanism in Unsaturated Polyester Resins. *Powder Technol.* **2019**, *354*, 71−81.

(3) He, J.; Zeng, W.; Shi, M.; Lv, X.; Fan, H.; Lei, Z. Influence of Expandable Graphite on Flame Retardancy and Thermal Stability Property of Unsaturated Polyester Resins/Organic Magnesium Hydroxide Composites. *J. Appl. Polym. Sci.* **2020**, *137*, 47881.

(4) Kolic, T. M.; Shen, L.; MacPherson, K.; Fayez, L.; Gobran, T.; Helm, P. A.; Marvin, C. H.; Arsenault, G.; Reiner, E. J. The Analysis of Halogenated Flame Retardants by GC-HRMS in Environmental Samples. *J. Chromatogr. Sci.* **2009**, *47*, 83−91.

(5) Shaw, S. D.; Blum, A.; Weber, R.; Kannan, K.; Rich, D.; Lucas, D.; Koshland, C. P.; Dobraca, D.; Hanson, S.; Birnbaum, L. S. Halogenated Flame Retardants: Do the Fire Safety Benefits Justify the Risks? *Rev. Environ. Health* **2010**, *25*, 261−305.

(6) Chen, Z.; Jiang, M.; Zhang, Q.; Yu, Y.; Sun, G.; Jiang, J. Synergistic Effect of Combined Dimethyl Methylphosphonate with Aluminum Hydroxide or Ammonium Polyphosphate Retardant Systems on the Flame Retardancy and Thermal Properties of Unsaturated Polyester Resin. *Int. J. Polym. Anal. Charact.* **2017**, *22*, 509−518.

(7) Rybiński, P.; Janowska, G. Influence Synergetic Effect of Halloysite Nanotubes and Halogen-Free Flame-Retardants on Properties Nitrile Rubber Composites. *Thermochim. Acta* **2013**, *557*, 24−30.

(8) Liu, J.; Zhang, Y.; Peng, S.; Pan, B.; Lu, C.; Liu, H.; Ma, J.; Niu, Q. Fire Property and Charring Behavior of High Impact Polystyrene Containing Expandable Graphite and Microencapsulated Red Phosphorus. *Polym. Degrad. Stab.* **2015**, *121*, 261−270.

(9) Jeencham, R.; Suppakarn, N.; Jarukumjorn, K. Effect of Flame Retardants on Flame Retardant, Mechanical, and Thermal Properties of Sisal Fiber/Polypropylene Composites. *Composites, Part B* **2014**, *56*, 249−253.

(10) Du, B.; Fang, Z. Effects of Carbon Nanotubes on the Thermal Stability and Flame Retardancy of Intumescent Flame-Retarded Polypropylene. *Polym. Degrad. Stab.* **2011**, *96*, 1725−1731.

(11) Zhang, J.; Manias, E.; Wilkie, C. A. Polymerically Modified Layered Silicates: An Effective Route to Nanocomposites. *J. Nanosci. Nanotechnol.* **2008**, *8*, 1597−1615.

(12) Ye, L.; Wu, Q.; Qu, B. Synergistic Effects and Mechanism of Multiwalled Carbon Nanotubes with Magnesium Hydroxide in Halogen-Free Flame Retardant EVA/MH/MWNT Nanocomposites. *Polym. Degrad. Stab.* **2009**, *94*, 751−756.

(13) Guo, K. Y.; Wu, Q.; Mao, M.; Chen, H.; Zhang, G. D.; Zhao, L.; Gao, J. F.; Song, P.; Tang, L. C. Water-Based Hybrid Coatings toward Mechanically Flexible, Super-Hydrophobic and Flame-Retardant Polyurethane Foam Nanocomposites with High-Efficiency and Reliable Fire Alarm Response. *Composites, Part B* **2020**, *193*, 108017.

(14) Pan, Y. H.; Zhao, Q. Y.; Gu, L.; Wu, Q. Y. Thin Film Nanocomposite Membranes Based on Imologite Nanotubes Blended Substrates for Forward Osmosis Desalination. *Desalination* **2017**, *421*, 160−168.

(15) Li, L.; Ma, W.; Takada, A.; Takayama, N.; Takahara, A. Organic-Inorganic Hybrid Films Fabricated from Cellulose Fibers and Imogolite Nanotubes. *Biomacromolecules* **2019**, *20*, 3566−3574.

(16) Arancibia-Miranda, N.; Escudey, M.; Molina, M.; García-González, M. T. Use of Isoelectric Point and PH to Evaluate the Synthesis of a Nanotubular Aluminosilicate. *J. Non-Cryst. Solids* **2011**, *357*, 1750−1756.

(17) Zanzottera, C.; Vicente, A.; Celasco, E.; Fernandez, C.; Garrone, E.; Bonelli, B. Physico-Chemical Properties of Imogolite Nanotubes Functionalized on Both External and Internal Surfaces. *J. Phys. Chem. C* **2012**, *116*, 7499−7506.

(18) Wan, M.; Shen, J.; Sun, C.; Gao, M.; Yue, L.; Wang, Y. Ionic Liquid Modified Graphene Oxide for Enhanced Flame Retardancy and Mechanical Properties of Epoxy Resin. *J. Appl. Polym. Sci.* **2021**, *138*, 50757.

(19) Amara, M. S.; Rouzière, S.; Paineau, E.; Bacia-Verloop, M.; Thill, A.; Launois, P. Hexagonalization of Aluminogermanate Imogolite Nanotubes Organized into Closed-Packed Bundles. *J. Phys. Chem. C* **2014**, *118*, 9299−9306.

(20) Otsuka, H.; Takahara, A.Structure and Properties of Imogolite Nanotubes and Their Application to Polymer Nanocomposites. In *Inorganic and Metallic Nanotubular Materials: Recent Technologies and Applications*; Kijima, T., Ed.; Springer Berlin Heidelberg: Berlin, Heidelberg, 2010; pp 169−190.

(21) Bertuoli, P. T.; Piazza, D.; Scienza, L. C.; Zattera, A. J. Preparation and Characterization of Montmorillonite Modified with 3-Aminopropyltriethoxysilane. *Appl. Clay Sci.* **2014**, *87*, 46−51.

(22) Donmez Cavdar, A. Effect of Various Wood Preservatives on Limiting Oxygen Index Levels of Fir Wood. *Meas.: J. Int. Meas. Confed.* **2014**, *50*, 279−284.

(23) Hu, C.; Fontaine, G.; Tranchard, P.; Delaunay, T.; Collinet, M.; Marcille, S.; Bourbigot, S. In-Situ Investigation of Temperature Evolution of Drippings via an Optimized UL-94 Instrumentation: Application to Flame Retarded Polybutylene Succinate. *Polym. Degrad. Stab.* **2018**, *155*, 145−152.

(24) Yuan, B.; Bao, C.; Qian, X.; Jiang, S.; Wen, P.; Xing, W.; Song, L.; Liew, K. M.; Hu, Y. Synergetic Dispersion Effect of Graphene Nanohybrid on the Thermal Stability and Mechanical Properties of Ethylene Vinyl Acetate Copolymer Nanocomposite. *Ind. Eng. Chem. Res.* **2014**, *53*, 1143−1149.

(25) Bai, Z.; Song, L.; Hu, Y.; Gong, X.; Yuen, R. K. K. Investigation on Flame Retardancy, Combustion and Pyrolysis Behavior of Flame Retarded Unsaturated Polyester Resin with a Star-Shaped Phosphorus-Containing Compound. *J. Anal. Appl. Pyrolysis* **2014**, *105*, 317−326.

(26) Lewin, M. Synergistic and Catalytic Effects in Flame Retardancy of Polymeric Materials—an Overview. *J. Fire Sci.* **1999**, *17*, 3−19.

(27) Jiang, M.; Zhang, Y.; Yu, Y.; Zhang, Q.; Huang, B.; Chen, Z.; Chen, T.; Jiang, J. Flame Retardancy of Unsaturated Polyester Composites with Modified Ammonium Polyphosphate, Montmorillonite, and Zinc Borate. *J. Appl. Polym. Sci.* **2019**, *136*, 47180.

(28) Chen, Z.; Yu, Y.; Zhang, Q.; Chen, Z.; Chen, T.; Li, C.; Jiang, J. Surface-Modified Ammonium Polyphosphate with (3-Aminopropyl) Triethoxysilane, Pentaerythritol and Melamine Dramatically Improve Flame Retardancy and Thermal Stability of Unsaturated Polyester Resin. *J. Therm. Anal. Calorim.* **2021**, *143*, 3479−3488.

(29) Schartel, B.; Bartholmai, M.; Knoll, U. Some Comments on the Use of Cone Calorimeter Data. *Polym. Degrad. Stab.* **2005**, *88*, 540−547.
(30) Makhlouf, G.; Hassan, M.; Nour, M.; Abdel-Monem, Y. K.; Abdelkhalik, A. Evaluation of Fire Performance of Linear Low-Density Polyethylene Containing Novel Intumescent Flame Retardant. *J. Therm. Anal. Calorim.* **2017**, *130*, 1031−1041.
(31) Tian, S.; He, H.; Wang, D.; Yu, P.; Jia, Y.; Luo, Y. Study of Using Aluminum Hypophosphite as a Flame Retardant for Low-Density Polyethylene. *Fire Mater.* **2017**, *41*, 983−992.
(32) Zuo, J.; Li, R.; Feng, S.; Liu, G.; Zhao, J. Flame Retardancy and Its Mechanism of Polymers Flame Retarded by DBDPE/Sb2O3. *J. Cent. South Univ. Technol.* **2008**, *15*, 64−68.
(33) Nazaré, S.; Kandola, B. K.; Horrocks, A. R. Smoke, CO, and CO2 Measurements and Evaluation Using Different Fire Testing Techniques for Flame Retardant Unsaturated Polyester Resin Formulations. *J. Fire Sci.* **2008**, *26*, 215−242.

https://doi.org/10.1021/acsomega.2c02803
ACS Omega 2022, 7, 47601−47609